ELSEVIER

Progress in Organic Coatings 49 (2004) 74–83

PROGRESS IN ORGANIC COATINGS

www.elsevier.com/locate/porgcoat

Optical properties of an eccentrically located pigment within an air bubble

Jean-Claude Auger [a,*], Rubén G. Barrera [b], Brian Stout [c]

[a] *Centro de Investigación en Polímeros, Grupo COMEX, Blvd Manuel Avila Camacho No. 138, Lomas de Chapultepec, 11560 Mexico DF, Mexico*
[b] *Instituto de Física de la Universidad Nacional Autónoma de México, Apartado Postal 20-364, 01000 Mexico DF, Mexico*
[c] *Institut Fresnel UMR 6133, Faculté des Sciences et Techniques, Centre de Saint Jeróme, 13397 Marseilles Cedex 20, France*

Received 28 February 2003; accepted 26 August 2003

Abstract

We study the orientational average of the scattering efficiencies of scatterers composed by an eccentrically located spherical TiO_2 pigment within an air bubble embedded in resin. This study is carried out within a general T-matrix formalism and takes into account the contributions of the asymmetry parameter to the photon transport mean-free path. We perform a detailed comparison of the scattering efficiency of this system with the one corresponding to the same pigment particle embedded directly in resin. We showed that placing a TiO_2 pigment eccentrically into an air bubble embedded in resin could not increase the scattering efficiency of the pigment in comparison to a system consisting of the same fractional volume of pigment particles and the same fractional volume of air bubbles acting independently within the same resin.

Keywords: Optical properties; Pigment; Eccentrically

1. Introduction

Opacity, also called hiding power, is an important optical property of white-paint coatings. It describes their capability to hide a substrate to the human eye. The main ingredient of a white coating is the pigment, and it usually consists of TiO_2 (rutile) crystallites embedded in a non-absorbing resin. These crystallites are also non-absorbing in most of the visible range, and scatter light very strongly. Therefore, the incident light undergoes an efficient process of multiple scattering, which in absence of absorption and for a sufficiently thick film, will yield complete hiding, that is, all the incident light will be eventually reflected backwards. The requirement that the pigment should be non-absorbing is related to the whiteness of the coating. It is well known that small additions of black pigment to a white paint will contribute to a larger hiding, however, it will make it look gray.

A simple way to picture the interaction of light with a white coating is to regard the multiple-scattering phenomenon as the diffusion of photons through a random arrangement of scatterers, and to borrow the concepts used in kinetic theory of transport. Within this picture, the photon mean-free path l_S, is defined as the average travel distance of the photon between two scattering events, and is inversely proportional to the number density of scattering particles times their scattering cross-section. The thickness of the system (coating film), measured in units of mean-free paths is known as the optical thickness, and for the diffusion picture to be valid the optical thickness should much greater than one.

Consequently, in a coating of a given thickness, one could enhance multiple scattering (photon transport) by minimizing, for example, the photon mean-free path, that is, by preparing a concentrated mixture of strong scatterers. The strength of the scattering is measured by the size of the scattering cross-section per unit volume, and this usually increases with the contrast in the index of refraction between the pigment and the resin, and shows resonance peaks as a function of the size and shape of the scatterers.

However, the transfer of radiation through multiple scattering in a system of randomly located spheres depends not only on the size of the scatterer (total cross-section) but also on its angular distribution (differential cross-section). The size parameter, defined as the circumference of the particle divided by the wavelength of the incident radiation, determines the angular distribution of the scattering, and the effects of this angular distribution in the transport of photons are taken into account through the so called asymmetry parameter. This parameter serves to define the photon transport mean-free path l_T, and the transport cross-section, which are the relevant parameters in transport theory. As the size

* Corresponding author.
E-mail address: jcauger@cip.org (J.-C. Auger).

0300-9440/$ – see front matter © 2003 Published by Elsevier B.V.
doi:10.1016/j.porgcoat.2003.08.013

parameter increases, the angular distribution of the scattering is directed more towards the forward direction yielding an increase in the transport mean-free path and a decrease in the reflectance, for a given filling fraction of particles. Nevertheless, the reflectance will tend to 1 for a non-absorbing system with thickness much larger than the transport mean-free path, that is, all the scattered light will eventually come back.

For non-absorbing particles with size parameter of the order or greater than 1, the transport scattering cross-section per unit volume as a function of the radius of particles, starts growing as the volume of the particles, then displays a resonant structure and for large particles it decays as the inverse of the radius. Therefore, each pigment should have an optimum size to maximize opacity for a fixed wavelength. In the case of rutile, the diameter turns out to be around 0.25 μm. One can recall that in case of a colored paint, absorption phenomena contribute also to opacity. To some extent, the shape of the pigment particles can also have an influence on the scattering and absorption properties of the pigment. In this work, we will consider only white paint with spherical pigment particles.

Due to the large value of the refractive index of rutile (around 2.8) and its transparency in the visible range, rutile particles with a size of 0.25 μm are the most effective pigment in white-paint fabrication. However, due to its high cost, which can reach up to 40% of the total cost in a paint formulation, the coating industry has been forced to investigate plausible alternatives for its total, or at least partial substitution. Within this perspective, it has been proposed to use air bubbles as a pigment. This kind of product already exists in the market with the commercial name of Rhopaque. In this product, the air bubbles are encapsulated in a hard polymer resin. However, since the contrast between the index of refraction of air (=1) and the resin (around 1.5) is smaller than the one between resin and rutile (around 2.8), the air bubbles scatter light much less efficiently than rutile.

Consequently, the substitution of rutile by air cannot be total, and its use is also limited by the total amount of solids that a paint can sustain. Therefore, encapsulated air bubbles are not the definitive solution for the substitution of rutile. However, since rutile scatters more in air than in the resin due to a higher contrast in index of refraction, it has been suggested to place the rutile crystallites in the encapsulated air bubble in order to increase their scattering efficiency.

The first theoretical study on this system was made by Ross [1] and Kerker et al. [2] at the beginning of the seventies. They calculated the scattering efficiency of system composed by a spherical particle of rutile placed at the center of spherical air bubble surrounded by a boundless medium of polymer resin. They showed that due to the interference of the fields radiated by the pigment and the induced charge at the air–resin interface, the encapsulated pigment could never scatter light with a greater efficiency than the optimum size isolated pigment embedded directly into the resin (Fig. 1a).

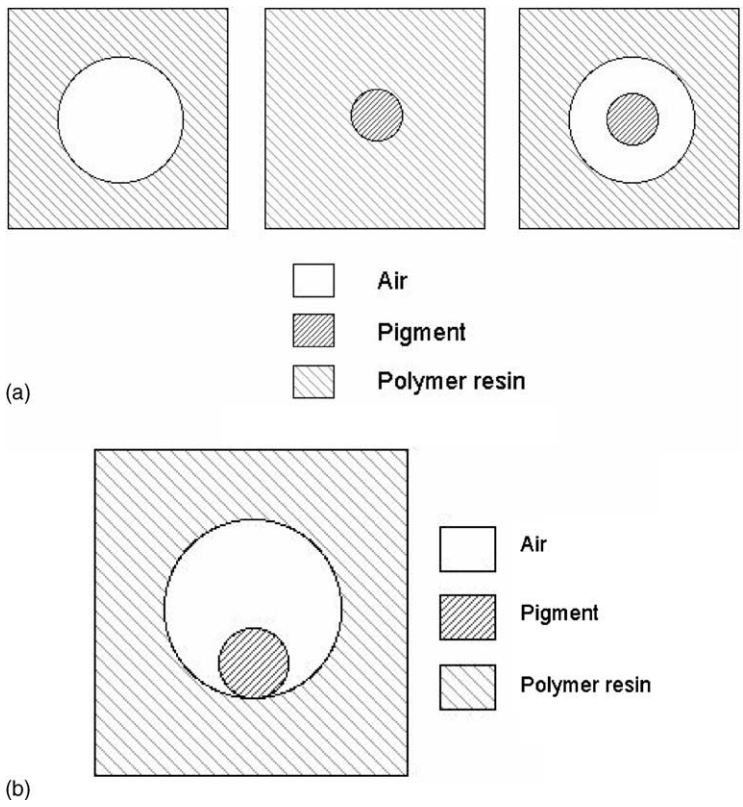

Fig. 1. Different systems under study—air bubble and TiO_2 pigment isolated into the resin: system of TiO_2 pigment located at (a) the center of the air bubble and (b) the inner surface of the air bubble, surrounded by the polymer resin.

Nevertheless, Ross and Kerker pointed out two distinctive phenomena: (i) for small size parameters of the air bubble and some specific size of the pigment, the scattering efficiency of the encapsulated system could come close to 0, optically speaking the system would not be seen; they call this invisibility, and (ii) for large size parameters of the air bubble, and some specific sizes of the pigment, the encapsulated system could scatter more than the air bubble and the pigment isolated separately within the resin; they call this a synergetic effect. However, due to the lack of theoretical tools and computer power at that time, the calculations were only performed placing the pigment right at the center of the air bubble. Obviously, due to gravity or sticking forces, it is not likely to expect that the TiO_2 particle would be located precisely at the center of the bubble.

In this work, we propose a more realistic study of the optical parameters of the systems analyzed by Kerker assuming that the pigment is stuck at the internal face of the air bubble (Fig. 1b). Besides complicating the theoretical formalism by breaking the spherical symmetry of the concentric system, one should evaluate the average of the optical parameters over all possible positions of the pigment on the internal surface of the air bubble. Indeed, this averaging procedure simply recognizes that the position of the pigment cannot be controlled and would be randomly located on the internal side of the air bubble.

Kerker also studied the strength of the synergetic effect, by comparing the scattering properties of the concentric system with those of a system composed of the same pigment, and the same air bubble but acting independently within the resin. This comparison has a limited validity in paint formulation because in the systems that are compared the fractional volume of the pigments are different. Indeed, since the fraction of solids in paints is one of the main control parameters, the scattering properties of different pigments must be compared in systems with equivalent fractional volumes. Therefore, in our study here we compare the scattering properties of a system with the pigment eccentrically located on the inner face of the air bubble, simply called the eccentric system, with a system consisting of an identical volume of pigment particles and a certain volume of air bubbles acting independently within the resin; the volume of the air bubbles is determined by demanding that the total volume occupied by the scatterers (pigment plus air bubbles) is the same as the volume occupied by the bubbles in the eccentric system.

2. Theory

2.1. Scattering by a homogeneous dielectric sphere

The analytical solution of Maxwell's equations for the scattering of a monochromatic plane wave by a spherical particle, embedded in an infinite non-absorbing media, was first developed by Mie [3]. It was later extended to an arbitrarily shaped particle [4–6] using a T-matrix formalism. The fundamental procedure in both approaches can be summarized as follows: one considers the scattering of a monochromatic plane wave of frequency ω and wavevector k_0 by a spherical dielectric particle of radius a_1 embedded in a homogeneous non-absorbing matrix. The indices of refraction of the sphere and the medium are N_1 and N_0.

The incident, scattered and internal fields, denoted by $\mathbf{E}_{\mathrm{inc},1}$, $\mathbf{E}_{\mathrm{sca},1}$ and $\mathbf{E}_{\mathrm{int},1}$, respectively, are expanded on the vectorial spherical wave basis $\boldsymbol{\Psi}^{(1)}_{\sigma nm,1}$ and $\boldsymbol{\Psi}^{(3)}_{\sigma nm,1}$ as:

$$\mathbf{E}_{\mathrm{inc},1} = E_0 \sum_{\sigma=1}^{2} \sum_{n=1}^{\infty} \sum_{m=-n}^{n} a_{\sigma nm} \boldsymbol{\Psi}^{(1)}_{\sigma nm,1}(k_0 \mathbf{r}) \tag{1}$$

$$\mathbf{E}_{\mathrm{sca},1} = E_0 \sum_{\sigma=1}^{2} \sum_{n=1}^{\infty} \sum_{m=-n}^{n} f_{\sigma nm} \boldsymbol{\Psi}^{(3)}_{\sigma nm,1}(k_0 \mathbf{r}) \tag{2}$$

$$\mathbf{E}_{\mathrm{int},1} = E_0 \sum_{\sigma=1}^{2} \sum_{n=1}^{\infty} \sum_{m=-n}^{n} b_{\sigma nm} \boldsymbol{\Psi}^{(1)}_{\sigma nm,1}(k_1 \mathbf{r}) \tag{3}$$

where $\mathbf{r}$ is the position vector and E_0 the amplitude of the incident plane wave with wavelength λ_0 and wavevector $k_0 = 2\pi/\lambda_0 N_0$. The superscripts (1) and (3) indicate that the radial dependence of the corresponding vectorial waves is either a spherical Bessel function $j_n(kr)$ or a spherical Hankel function $h_n^{(1)}(kr)$, respectively. The subscript 1 means that the origin of the basis is located at the geometrical center of the sphere defined in O_1.

Using the boundary conditions for the electromagnetic fields at the surface of the sphere yields a linear system of equations which couples the coefficients $a_{\sigma nm}$, $f_{\sigma nm}$ and $b_{\sigma nm}$. Eliminating the internal field coefficients $b_{\sigma nm}$, allows one to express directly the unknown scattered-field coefficients $f_{\sigma nm}$ as function of the known incident-field coefficients $a_{\sigma nm}$, through a matrix relation $\mathbf{f} = \bar{\mathbf{T}} \cdot \mathbf{a}$, where $\bar{\mathbf{T}}$ is a diagonal matrix, usually called the T-matrix.

The elements of the T-matrix in this spherical representation depend on the radius a_1 of the sphere and the magnitude of the wavevectors in the matrix k_0 and in the sphere $k_1 = k_0 N_1/N_0$ (see Appendix A). They are independent of the orientation and polarization of the incident wave, thus they represent an intrinsic property of the scattering system. Once the T-matrix and the $f_{\sigma nm}$ coefficients are evaluated, Eq. (2) yields an explicit analytical expression of the scattered field. Also, with this procedure, quantities like the total scattering and extinction cross-sections or the elements of the scattering matrix, can be calculated.

2.2. Scattering by a concentrically arranged dielectric sphere

The analytical solution of the scattering by a *concentrically arranged* sphere, i.e. a dielectric sphere containing a concentric spherical inclusion of radius a_2, and complex index of refraction N_2, was performed by Kerker [7]. The incident and scattered fields can be expressed as in Eqs. (1)

and (2), while the general form of the electric field in the region internal to the host and external to the inclusion is a superposition of incoming and outgoing spherical waves. The analytical expression for the field $\mathbf{E}_{\mathrm{int},1}$ in this region is thus given by

$$\mathbf{E}_{\mathrm{int},1} = E_0 \sum_{\sigma=1}^{2} \sum_{n=1}^{\infty} \sum_{m=-n}^{n} \times [e_{\sigma nm} \boldsymbol{\Psi}^{(3)}_{\sigma nm,1}(k_1\mathbf{r}) + g_{\sigma nm} \boldsymbol{\Psi}^{(4)}_{\sigma nm,1}(k_1\mathbf{r})] \quad (4)$$

where the superscript (4) means that the radial dependence of the corresponding wave depends on the spherical Hankel function $h_n^{(2)}(kr)$.

The internal field of the inner inclusion has the same kind of expansion as that given in Eq. (3), but taking into account the fact that the wavevector in the inclusion is defined by $k_2 = k_0 N_2/N_0$, that is,

$$\mathbf{E}_{\mathrm{int},2} = E_0 \sum_{\sigma=1}^{2} \sum_{n=1}^{\infty} \sum_{m=-n}^{n} p_{\sigma nm} \boldsymbol{\Psi}^{(1)}_{\sigma nm,2}(k_2\mathbf{r}) \quad (5)$$

where the subscript 2 means that the coordinate system has its origin located at the geometrical center of the inclusion defined in O_2. In this case, it does not add any further complications because the center of the inclusion O_2 coincides with the center of the sphere O_1.

Using the boundary condition for the fields on the host and inclusion interfaces, yields two linear systems of coupled equations involving the coefficients $a_{\sigma nm}$, $f_{\sigma nm}$, $e_{\sigma nm}$, $g_{\sigma nm}$ and $p_{\sigma nm}$. Solving these linear systems, one obtains the matrix relation $\mathbf{f} = \bar{\mathbf{T}} \cdot \mathbf{a}$, where $\bar{\mathbf{T}}$ is the diagonal T-matrix of the *concentric* system. The analytical expressions of its elements are given in Appendix A.

2.3. Scattering by an sphere containing a spherical eccentric inclusion

The first study on the scattering of light by a host sphere containing an eccentric spherical inclusion were first performed by Borghese et al. [8], and later on by Videen et al. [9] and Ngo et al. [10]. In those studies, the position of the inclusion was limited to lie along the *Oz* axis. We extended this analytical solution to an arbitrary location of the inclusion using a T-matrix approach [11]. Below, we recall briefly the fundamental equations of this formalism.

The incident, scattered and internal fields of the host sphere, denoted by $\mathbf{E}_{\mathrm{inc},1}$, $\mathbf{E}_{\mathrm{sca},1}$ and $\mathbf{E}_{\mathrm{int},1}$, respectively, are expanded in the coordinate system centered in O_1, yielding the expressions given by Eqs. (1), (2) and (4). The difficulty now is that the inclusion is located at an arbitrary position denoted by (r_0, θ_0, ϕ_0) in the spherical coordinate system of the host. In order to impose boundary conditions at the interface of the inclusion, it is necessary to expand the incident, scattered and internal fields of the inclusion in a second basis centered at O_2. The internal field of the inclusion, however, has the expression given by Eq. (5), and the expression of the field external to the inclusion, which is a superposition of incoming and outgoing spherical waves, is now given by the expression:

$$\mathbf{E}_{\mathrm{ext},2} = E_0 \sum_{\sigma=1}^{2} \sum_{n=1}^{\infty} \sum_{m=-n}^{n} \times [r_{\sigma nm} \boldsymbol{\Psi}^{(3)}_{\sigma nm,2}(k_1\mathbf{r}) + t_{\sigma nm} \boldsymbol{\Psi}^{(4)}_{\sigma nm,2}(k_1\mathbf{r})] \quad (6)$$

Applying the boundary conditions at the interfaces of the inclusion and the host, yields two linear systems of coupled equations between the $r_{\sigma nm}$, $t_{\sigma nm}$, $p_{\sigma nm}$ and $a_{\sigma nm}$, $f_{\sigma nm}$, $e_{\sigma nm}$, $g_{\sigma nm}$ coefficients. The first set of equations leads to $\mathbf{r} = \bar{\mathbf{Q}} \cdot \mathbf{t}$, where the coefficients of the $\bar{\mathbf{Q}}$ matrix are given in Appendix A. It is clear that $\mathbf{E}_{\mathrm{ext},2}$ and $\mathbf{E}_{\mathrm{int},1}$ describe the field in the same region of space, and in fact they describe the same fields, but with field expansions in two different basis sets. In order to replace $r_{\sigma nm}$ by $e_{\sigma nm}$ and $t_{\sigma nm}$ by $g_{\sigma nm}$ one must express the basis vector of the inclusion $\boldsymbol{\Psi}^{(q)}_{\sigma nm,2}$ in terms of the basis vector of the principal coordinate system, $\boldsymbol{\Psi}^{(q)}_{\sigma nm,1}$. This translation is performed with the aid of the translation theorem of the vectorial spherical wave functions introduced by Stein [12]. Truncating now the infinite multipole expansion to the first $n = N_{\max}$ orders, and after some algebra, one finds that the two linear systems lead to one set of $8N_{\max}(N_{\max} + 2)$ equations which relate the components of the vectors **a**, **f** and **t** corresponding to the incident, scattered and internal field, respectively. Eliminating the components of the internal field, one finds

$$\mathbf{f} = \bar{\mathbf{D}} \cdot \bar{\mathbf{M}}^{-1} \cdot \mathbf{a} \equiv \bar{\mathbf{T}} \cdot \mathbf{a} \quad (7)$$

where $\bar{\mathbf{T}}$ is now the T-matrix of the entire system composed of a dielectric spherical particle containing a spherical dielectric eccentric inclusion. The matrices $\bar{\mathbf{M}}$ and $\bar{\mathbf{D}}$ are defined by $\mathbf{a} = \bar{\mathbf{M}} \cdot \mathbf{b}$ and $\mathbf{f} = \bar{\mathbf{D}} \cdot \mathbf{b}$, and explicit expressions for their components are given in Appendix A.

We remind the reader that although the T-matrix formalism involves an infinite expansion of the electric and magnetic fields on the partial spherical wave basis, for finite sized particles, only a finite number of coefficients are non-negligible. Therefore, the infinite-series expression for the electromagnetic fields can be truncated at an order $N_{\max}$, which is defined as the maximum value of n after which the series converges. The order of truncation depends on the size parameter of the particle, and Wiscombe's criterion [13] is used to give an upper bound for $N_{\max}$.

2.4. Scattering parameters

The scattering parameters of an homogeneous, concentric or eccentric system can be evaluated once the T-matrix and the scattering fields coefficients of the systems are known. One of the main parameter in scattering theory is the scattering cross-section C_{sca}, which measures the strength of the scattering process, and is defined as the total power scattered

by the sphere over the incident flux. C_{sca} has the units of area, and for particles large with respect to the wavelength of the incident direction, it has a limiting value of twice the geometrical projected area. The analytical expression for C_{sca} in the T-matrix formalism is given by

$$C_{sca} = \frac{1}{k_0^2}\sum_{\sigma=1}^{2}\sum_{n=1}^{\infty}\sum_{m=-n}^{n}|f_{\sigma nm}|^2 \tag{8}$$

The opacity of a white coating, however, depends not only on the strength of the scattering process, but also on the angular distribution of the scattered radiation. A parameter that helps to measure the magnitude of the angular distribution is the asymmetry parameter g, defined as

$$g = \frac{1}{C_{sca}}\int_0^{2\pi}\int_0^{\pi}\frac{dC_{sca}}{d\Omega}\cos\theta\, d\Omega \tag{9}$$

where $dC_{sca}/d\Omega$ is the differential scattering cross-section (scattering cross-section per unit solid angle). One can see that g takes values from 1 to -1, corresponding to the limiting cases where all the radiation is either scattered in the forward or in the backward direction, respectively, while isotropic scattering has $g = 0$. In our formalism the analytical expression of the asymmetry parameter in Eq. (9) is given by

$$g = \frac{1}{k_0^2 C_{sca}}\mathrm{Re}[\mathbf{f}^{\dagger}\cdot\bar{\boldsymbol{\gamma}}\cdot\mathbf{f}] \tag{10}$$

where the matrix $\bar{\boldsymbol{\gamma}}$ has the form

$$\bar{\boldsymbol{\gamma}} = \begin{bmatrix} \Xi & \Theta \\ \Theta & \Xi \end{bmatrix}$$

with

$$\Theta_{nm,\nu\mu} = \frac{m}{n(n+1)}\delta_{m,\mu}\delta_{n,\nu},$$

$$\Xi_{nm,\nu\mu} = \frac{i\delta_{m,\mu}}{\sqrt{(2n+1)(2\nu+1)}} \times \left(\frac{\delta_{n-1,\nu}}{n}\sqrt{(n^2-1)(n^2-m^2)} - \frac{\delta_{\nu,n+1}}{\nu}\sqrt{(\nu^2-1)(\nu^2-m^2)}\right) \tag{11}$$

The result of Eq. (10) is valid only when the incident wavevector is parallel to the Oz axis. In order to characterize the general scattering efficiency of a pigment, one invokes the scattering coefficient S, defined as the inverse of the transport mean-free path:

$$S = f_p s \equiv f_p\frac{C_{sca}}{v}(1-g) \tag{12}$$

where f_p is the volume filling fraction of the pigment and v the volume of a single pigment inclusion. One can see that for a fixed volume concentration of pigment, the optimum scattering coefficient S can be attained by simultaneously maximizing C_{sca}/v and minimizing g.

In a previous work [11], we studied an eccentrically located TiO_2 pigment within an air bubble but our calculation was restricted only to the average scattering cross-sections per unit volume. As mentioned in Section 1, however, the total scattering cross-section gives limited information on the light transport within the scattering system, since this quantity by itself does not take into account the angular distribution of the scattered intensity, which is taken into account by g. Furthermore, a relevant study of the usefulness of the eccentric system in the formulation of paints, must consider the properties of the scattering coefficient S averaged over all possible orientations related to the location of the pigment.

In order to avoid the difficulties related to an analytical derivation of the orientational average $\langle s\rangle_\theta$ of the scattering parameter [6], which involves the rotational theorem of the spherical wave functions, we perform instead a straightforward numerical average. We first evaluate the scattering coefficient for different locations of the inclusion, but since the average should be independent of ϕ, we take $\phi = 0$, and numerically integrate over different values of θ. We then perform the average over all these different locations, and also over two orthogonal field polarizations, i.e.

$$\langle S\rangle_\theta = \frac{1}{2V}\frac{\sum_{i=1}^{i=N}\sum_{j=1}^{j=2}C_{sca}^{i,j}(1-g^{i,j})\sin\theta_i\,\Delta\theta}{\sum_{i=1}^{i=N}\sin\theta_i\,\Delta\theta} \tag{13}$$

where $j = 1, 2$ for TE and TM polarizations, respectively. $C_{sca}^{i,j}$ and $g^{i,j}$ are, respectively, the scattering cross-section and the asymmetry parameter for a fixed location i of the inclusion and a fixed polarization j of the incident field. Each term in the sum is weighted by the factor $\sin\theta$, to take into account the assumption of equal probability at each azimuthal angle.

In order to check the numerical accuracy of Eq. (13), we compare the analytical orientational average of the scattering cross-section given by $\langle C_{sca}\rangle_\theta = 2\pi\,\mathrm{Re}\{\mathrm{Tr}[\bar{\mathbf{T}}^{\dagger}\cdot\bar{\mathbf{T}}]\}/k_0^2$ [14], with the corresponding numerical average for different values of $\Delta\theta$, that is,

$$\langle C_{sca}\rangle_\theta = \frac{1}{2}\frac{\sum_{i=1}^{i=N}\sum_{j=1}^{j=2}C_{sca}^{i,j}\sin\theta_i\Delta\theta}{\sum_{i=1}^{i=N}\sin\theta_i\,\Delta\theta} \tag{14}$$

We found that for $\Delta\theta = 10^\circ$, the numerical and analytical evaluations of $\langle C_{sca}\rangle_\theta$ had similar values up to the fifth decimal figure. We presume that the evaluation of $\langle S\rangle_\theta$ in Eq. (13) should be as accurate as $\langle C_{sca}\rangle_\theta$ for the same value of $\Delta\theta$.

3. Results and discussion

First we display the value of the orientation average of the scattering parameter $\langle S\rangle_\theta$, given in Eq. (13), as a function of the radius of the air bubble and the filling fraction p of the TiO_2 pigment. We have chosen the values of the radius to run between 0.116 and 0.323 μm, and the values of p to vary between 0 (pure air bubble) and 1 (pure pigment).

Throughout this study, the wavelength of the incident radiation is taken to be 0.546 μm. The indices of refraction for air, resin and TiO_2 are taken as 1.0, 1.51 and 2.97, respectively. These latter values are the one taken by Ross [1]. Fig. 2a and b represent the scattering efficiencies of the eccentric and concentric systems, whereas Fig. 2c represents the system composed of the TiO_2 pigment particles and the air bubbles acting independently. We will refer to these systems by $\langle S_a \rangle_\theta$, $\langle S_b \rangle_\theta$ and $\langle S_c \rangle_\theta$, respectively. The scattering efficiency of the isolated TiO_2 pigment embedded in the resin reaches its maximum of 17.84 μm^{-1} for radii between 0.090 and 0.092 μm.

The first important observation of this work is that the encapsulated eccentric pigment never scatters light with a higher efficiency than an optimum-sized pigment particle embedded directly in the resin, as in the case of the concentric system. Moreover, $\langle S_a \rangle_\theta$ exhibits a dramatic decrease compared to $\langle S_c \rangle_\theta$ throughout all values of p and r_1 under study. This decrease becomes stronger as the size of the air bubble increases. Also, when the size of the inclusion is close to the optimum size of the a single TiO_2 pigment particle, the scattering efficiency of the concentrically arranged system is increased, but it is still quite small compared to the efficiency of S_c.

In order to give a more detailed account of the quantitative difference of the scattering efficiencies of the three different systems mentioned above, Fig. 2d and e display a 2D plot of a cut in the 3D graphs shown in Fig. 2a–c. The radius of the air bubble is fixed at 0.122 and 0.300 μm, respectively. One can clearly see that the concentric and eccentric systems have a very similar variation, independently of the dimension of the air bubble, but with an magnitude much lower than the optimum size of the TiO_2 pigment.

The faint scattering efficiency of the eccentric system can be mainly attributed to two causes. The first, is that the size of the air bubble is smaller than the wavelength λ_0 in air, so there is actually no wave propagation within the air bubble. The main concept of the study was taken from the fact that TiO_2 pigment have a better scattering efficiency in air than in a polymeric resin. However, this result was obtained by assuming that the pigment is embedded in a infinite medium. Here, this is clearly not the case. Furthermore, the complexity of the fields in encapsulated region results in destructive interferences between the incoming and outgoing fields. The consequence of these destructive interferences is weakly scattered fields which leads to a small scattering efficiency of a coated system of spheres. The second explanation is that in order to optimize S, one should minimize g and optimize C_{sca}/V. However, it is well known that at least for spherical particles, as the size parameter increases, C_{sca}/V decreases and g increases, resulting in a small scattering efficiency amplitude of the composite system.

The other important result of this work is the analysis of the effect of the translation of the inclusion from the center of the air bubble to its inner interface. Comparing Fig. 2a and b, one can see that both systems have relatively the same scattering efficiency. We represented in Fig. 3 the different zones of scattering efficiency for each system, as a function of the radius of the air bubble r_1 and the filling fraction p. The black surfaces represent the zones where the concentrically arranged system has a greater scattering efficiency than the eccentric system, while the white zones represent the contrary. One can see that the eccentric pigment has, on the average, a larger C than the concentric system.

Indeed, the electromagnetic interactions between the inclusion and the air bubble increases as the pigment comes closer to the host surface. This can be shown by comparing the truncation index of the electromagnetic fields that is needed in order to obtain a numerical convergence of the scattering efficiency. Let us take N_{max} to be the truncation value of the n summation, for the concentric system, that is necessary to describe the scattering for a fixed size parameter of the air bubble and a fixed filling fraction p of the inclusion. Then, the corresponding truncation index necessary to describe the eccentric system, denoted by N'_{max}, will become $N'_{max} > N_{max}$. One should notice that an increase in the interactions does not always reflect an increase of the overall scattering efficiency, but on the average this is the case.

The concentrically arranged system has a larger $\langle S \rangle_\theta$ mainly when the size of the inclusion is close to the optimum size of TiO_2 in the resin. This could be due to modes of resonance that exist around this size and which can be better amplified when the inclusion is placed at the center of the host cavity. When the inclusion is shifted, the symmetry is broken, and the effect disappears.

The fact that both systems have a similar value of their scattering efficiency can be explained by the following reasoning: for a small value of p, both configurations are very different because the difference between the position of the inclusion in the concentric and eccentric system is very large (r_0 is comparable to r_1). This change of configuration could create a large difference in the scattering efficiency. However, the size of the particle is so small that, independent of the position of the inclusion, the scattering efficiencies of both system are close to the scattering efficiency of the air bubble alone, and do not greatly differ from one another. When p has a value close to unity, the size of the inclusion is comparable to the size of air bubble and the effect of the pigment should be considerable. However, in this case the shift in the position of the inclusion between both configurations is quite small, and the scattering efficiency of both systems remains comparable.

The last important result of this work is the study of the "synergetic effects" observed by Kerker. We recall that these effects appear when the concentric system has a larger scattering efficiency than the system with the air bubble and the pigment particles acting independently within the resin. One should notice that those effects are linked to the parameter $\langle S \rangle_\theta$, and they no longer exist if one compares the differences in C_{sca}/V in our study.

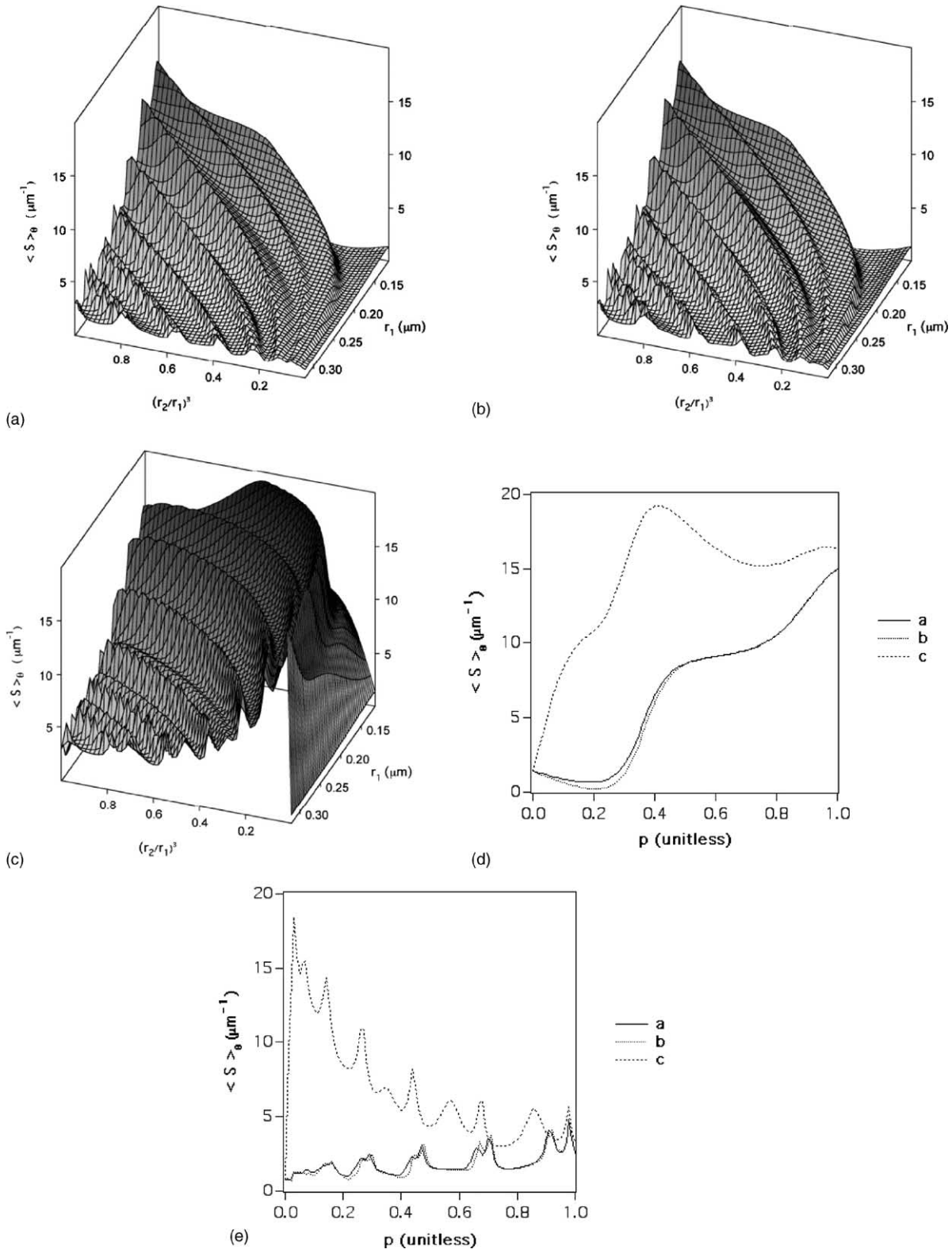

Fig. 2. Orientational averaged scattering efficiency, noted: (a) $\langle S_a \rangle_\theta$ of the system composed by the TiO_2 pigment located at the inner interface of the air bubble; (b) $\langle S_b \rangle_\theta$ of the system composed by the TiO_2 pigment located at the center of the air bubble; (c) $\langle S_c \rangle_\theta$ of the system composed by the isolated TiO_2 pigment and the air bubble as function of the radius of the air bubble (r_1) and the filling fraction $(r_1/r_2)^3$. (d) and (e) Orientational averaged scattering efficiency of the systems composed by: (a) the TiO_2 pigment located at the inner interface of the air bubble, (b) the TiO_2 pigment located at the center of the air bubble, (c) the isolated TiO_2 pigment and the isolated air bubble, as function of the filling fraction $p = (r_1/r_2)^3$. The radius of the air bubble is constant and set to $r_1 = 0.122$ and 0.300 μm, respectively.

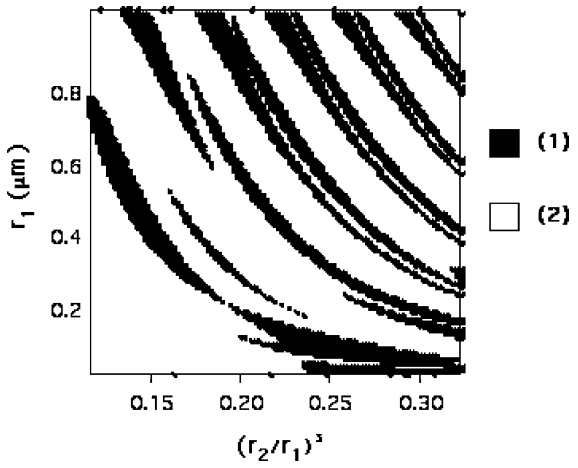

Fig. 3. Relative values $\langle S_b\rangle/\langle S_c\rangle$ of the scattering efficiency as a function of the radius of the air bubble r_1 and the filling fraction p. The black surfaces represent the zones where the concentric system has a greater scattering efficiency than the eccentric system ($\langle S_b\rangle_\theta > \langle S_a\rangle_\theta$), while the white zones represent the contrary ($\langle S_b\rangle_\theta < \langle S_a\rangle_\theta$).

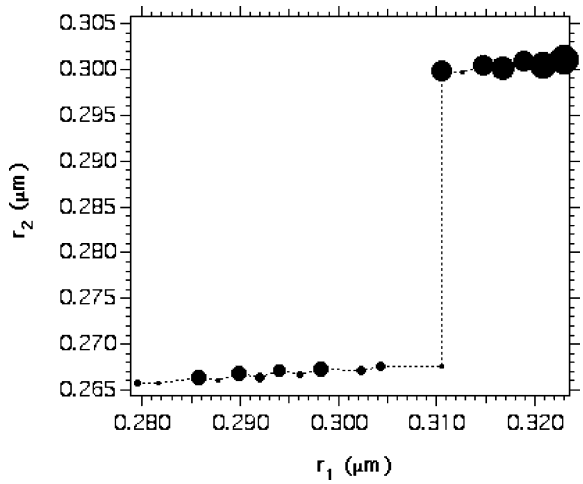

Fig. 5. Relative values $\langle S_b\rangle/\langle S_c\rangle$ as function of the radius of the air bubble and the radius of the inclusion r_2 at which the synergetic effect occurs. The size of the circles is proportional to the amplitude of $\langle S_b\rangle/\langle S_c\rangle$ which has a maximum value of 1.13.

The synergetic phenomena start at relatively large sizes of the air bubble ($a \approx 0.280\,\mu m$) and for large filling fractions ($p \approx 0.65$) when the eccentric and the system composed by the pigment particles and air bubbles acting independently have a very similar scattering efficiency. For smaller sizes of the air bubble and smaller value of the filling fraction p, the difference between the $\langle S\rangle_\theta$ for both system is huge, and there is no synergetic effect. We have plotted the relative values $\langle S_b\rangle/\langle S_c\rangle$ as function of the radius of the air bubble and the filling fraction p (Fig. 4) and the radius of the inclusion r_2 (Fig. 5) at which the synergetic effect occurs. The size of the circles in the plot is proportional to the amplitude of $\langle S_b\rangle/\langle S_c\rangle$ which has a maximum value of 1.13 in our range of calculation. One can see that there is a certain correlation between the relative size of the air bubble and the pigment for the synergetic effects. However, in order to make a more complete study of this phenomenon, one should increase the range of the size parameters under study.

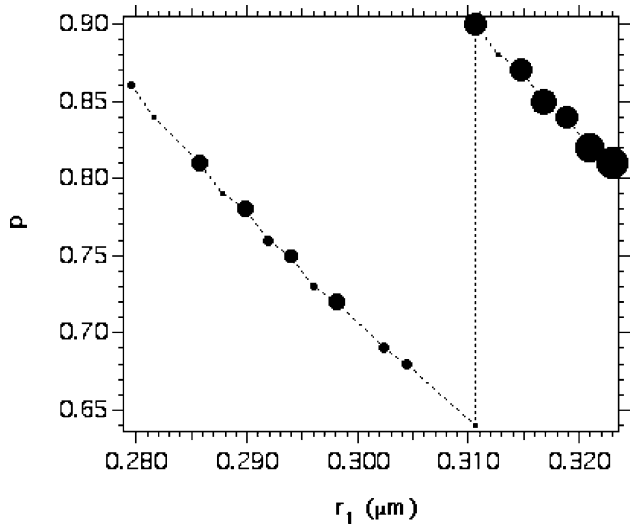

Fig. 4. Relative values $\langle S_b\rangle/\langle S_c\rangle$ as function of the radius of the air bubble and the filling fraction p at which the synergetic effect occurs. The size of the circles is proportional to the amplitude of $\langle S_b\rangle/\langle S_c\rangle$ which has a maximum value of 1.13.

4. Conclusion

We showed that placing a TiO_2 pigment eccentrically into an air bubble embedded in resin could not increase the scattering efficiency of the pigment in comparison to a system consisting of the same fractional volume of pigment particles and the same fractional volume of air bubbles acting independently within the same resin. In this case, one could not assume that the TiO_2 pigment was embedded in an infinite system. On the contrary, the path length covered by the wave in the air bubble was smaller than the extension of the wave itself. Consequently, the comparison with the scattering efficiency of a TiO_2 pigment in air cannot be applied. For a legitimate comparison in the scattering efficiency of these two systems one adjusts the filling fraction of the air bubbles so both systems have the same filling fraction of scatterers. We also showed that the scattering efficiency of the eccentric system was quite similar to the concentric system where the inclusion is placed at the center of the air bubble. We explained this result by showing that optically speaking both configurations were never very different.

Our study was performed for a fixed wavelength of the incident field and a limited range of radius for the air bubble. One could wonder if this range of sizes is representative enough. We showed that at least for spherical system, it seems that there is no need to extend the study for larger size of the air bubble because the scattering cross-section by unit volume will decrease proportionally while the asym-

metry parameter will increase. Also, extending the study to different wavelengths of the incident field to all the visible range, could probably change the different modes of resonance of the eccentric systems, changing the number and positions of the synergetic effects. However, the gap between the scattering efficiency of the eccentric system, and the optimum size of the TiO_2 pigment directly into the resin is so large that it not likely yield a change in the general tendency.

Finally, we mention that throughout this work, we have evaluated the scattering efficiency of independent scatterers. It is now well known that cooperative effects between scatters in a dense medium tends to decrease the scattering efficiency of the sum of the individual particles, thus the extrapolation of these results to non-isolated systems should be made with precaution.

Acknowledgements

The authors wish to acknowledge Eduardo Nahmad for the support given to this work. We also acknowledge the partial support of Consejo Nacional de Ciencia y Tecnología (México) and Centro de Investigación en Polimeros through grant RI-1200-2-1.

Appendix A. Analytical T-matrix coefficients

In the following formulae, we use $\psi_n(x) = xj_n(x)$, $\xi_n^{(1)} = xh_n^{(1)}(x)$, and a prime applied to these functions denotes a derivative with respect to the argument x.

A.1. Homogeneous spherical dielectric particle

The T-matrix is of the form

$$\begin{bmatrix} T^1_{\mathrm{HS}} & 0 \\ 0 & T^2_{\mathrm{HS}} \end{bmatrix}$$

where T^1 and T^2 are diagonal matrices whose matrix elements are given by $[T^1_{\mathrm{HS}}]_{nm,\nu\mu} = \delta_{n\nu}\delta_{m\mu}T^1_{\mathrm{HS},n}$, $[T^2_{\mathrm{HS}}]_{nm,\nu\mu} = \delta_{n\nu}\delta_{m\mu}T^2_{\mathrm{HS},n}$, with

$$T^1_{\mathrm{HS},n} = \left[\frac{k_1\psi_n(k_2a_2)\xi_n'^{(2)}(k_1a_2) - k_2\xi_n^{(2)}(k_1a_2)\psi_n'(k_2a_2)}{k_2\xi_n^{(1)}(k_1a_2)\psi_n'(k_2a_2) - k_1\psi_n(k_2a_2)\xi_n'^{(1)}(k_1a_2)}\right],$$

$$T^2_{\mathrm{HS},n} = \left[\frac{k_1\xi_n^{(2)}(k_1a_2)\psi_n'(k_2a_2) - k_2\psi_n(k_2a_2)\xi_n'^{(2)}(k_1a_2)}{k_1\psi_n(k_2a_2)\xi_n'^{(1)}(k_1a_2) - k_1\xi_n^{(1)}(k_1a_2)\psi_n'(k_2a_2)}\right]$$

Here, a_2 is the radius of the sphere and k_1 and $k_2 = k_1N_2/N_1$ are the magnitude of the wavevectors in the matrix and in the sphere, respectively.

A.2. Spherical dielectric particle containing a concentric dielectric spherical inclusion

The T-matrix is of the form

$$\begin{bmatrix} T^1_{\mathrm{CS}} & 0 \\ 0 & T^2_{\mathrm{CS}} \end{bmatrix}$$

where T^1 and T^2 are diagonal matrices whose matrix elements are given by $[T^1_{\mathrm{CS}}]_{nm,\nu\mu} = \delta_{n\nu}\delta_{m\mu}T^1_{\mathrm{CS},n}$, $[T^2_{\mathrm{CS}}]_{nm,\nu\mu} = \delta_{n\nu}\delta_{m\mu}T^2_{\mathrm{CS},n}$, with

$$T^1_{\mathrm{CS},n} = \left[\frac{B_n^{(1)} - B_n^{(2)}}{B_n^{(3)} - B_n^{(4)}}\right], \qquad T^2_{\mathrm{CS},n} = \left[\frac{C_n^{(1)} - C_n^{(2)}}{C_n^{(3)} - C_n^{(4)}}\right]$$

and

$$\begin{aligned}
B_n^{(1)} &= k_1\xi_n'^{(2)}(k_1a_2)[T^1_{\mathrm{HS}}\xi_n^{(1)}(k_2a_2) + \xi_n^{(2)}(k_2a_2)],\\
B_n^{(2)} &= k_2\xi_n^{(2)}(k_1a_2)[T^1_{\mathrm{HS}}\xi_n'^{(1)}(k_2a_2) + \xi_n'^{(2)}(k_2a_2)],\\
B_n^{(3)} &= k_2\xi_n^{(1)}(k_1a_2)[T^1_{\mathrm{HS}}\xi_n'^{(1)}(k_2a_2) + \xi_n'^{(2)}(k_2a_2)],\\
B_n^{(4)} &= k_1\xi_n'^{(1)}(k_1a_2)[T^1_{\mathrm{HS}}\xi_n^{(1)}(k_2a_2) + \xi_n^{(2)}(k_2a_2)]
\end{aligned}$$

$$\begin{aligned}
C_n^{(1)} &= k_1\xi_n^{(2)}(k_1a_2)[T^2_{\mathrm{HS}}\xi_n'^{(1)}(k_2a_2) + \xi_n'^{(2)}(k_2a_2)],\\
C_n^{(2)} &= k_2\xi_n'^{(2)}(k_1a_2)[T^2_{\mathrm{HS}}\xi_n^{(1)}(k_2a_2) + \xi_n^{(2)}(k_2a_2)],\\
C_n^{(3)} &= k_2\xi_n'^{(1)}(k_1a_2)[T^2_{\mathrm{HS}}\xi_n^{(1)}(k_2a_2) + \xi_n^{(2)}(k_2a_2)],\\
C_n^{(4)} &= k_1\xi_n^{(1)}(k_1a_2)[T^2_{\mathrm{HS}}\xi_n'^{(1)}(k_2a_2) + \xi_n'^{(2)}(k_2a_2)]
\end{aligned}$$

A.3. Spherical dielectric particle containing an eccentric dielectric spherical inclusion

The general expressions for the $\bar{\mathbf{M}}$ and $\bar{\mathbf{D}}$ matrix elements are given by:

$$\bar{\mathbf{M}} = \begin{bmatrix} \bar{M}^{nm(1,1)}_{\nu\mu} & \bar{M}^{nm(1,2)}_{\nu\mu} \\ \bar{M}^{nm(2,1)}_{\nu\mu} & \bar{M}^{nm(2,2)}_{\nu\mu} \end{bmatrix} \quad \text{and}$$

$$\bar{\mathbf{D}} = \begin{bmatrix} \bar{D}^{nm(1,1)}_{\nu\mu} & \bar{D}^{nm(1,2)}_{\nu\mu} \\ \bar{D}^{nm(2,1)}_{\nu\mu} & \bar{D}^{nm(2,2)}_{\nu\mu} \end{bmatrix} \tag{A.1}$$

where

$$\bar{M}^{nm(1,1)}_{\nu\mu} = A^{nm(1)}_{\nu\mu}\left[\frac{Z^{(c)}_{\nu n}\xi_n^{(1)}(k_0a_1) - (k_0/k_1)Z^{(a)}_{\nu n}\xi_n'^{(1)}(k_0a_1)}{\psi_n'(k_0a_1)\xi_n^{(1)}(k_0a_1) - \psi_n(k_0a_1)\xi_n'^{(1)}(k_0a_1)}\right],$$

$$\bar{M}^{nm(1,2)}_{\nu\mu} = B^{nm(1)}_{\nu\mu}\left[\frac{Z^{(d)}_{\nu n}\xi_n^{(1)}(k_0a_1) - (k_0/k_1)Z^{(b)}_{\nu n}\xi_n'^{(1)}(k_0a_1)}{\psi_n'(k_0a_1)\xi_n^{(1)}(k_0a_1) - \psi_n(k_0a_1)\xi_n'^{(1)}(k_0a_1)}\right],$$

$$\bar{M}^{nm(2,1)}_{\nu\mu} = B^{nm(1)}_{\nu\mu}\left[\frac{Z^{(a)}_{\nu n}\xi_n'^{(1)}(k_0a_1) - (k_0/k_1)Z^{(c)}_{\nu n}\xi_n^{(1)}(k_0a_1)}{\psi_n(k_0a_1)\xi_n'^{(1)}(k_0a_1) - \psi_n'(k_0a_1)\xi_n'^{(1)}(k_0a_1)}\right],$$

$$\bar{M}_{\nu\mu}^{nm(2,2)} = A_{\nu\mu}^{nm(1)} \left[\frac{Z_{\nu n}^{(b)} \xi_n'^{(1)}(k_0 a_1) - (k_0/k_1) Z_{\nu n}^{(d)} \xi_n^{(1)}(k_0 a_1)}{\psi_n(k_0 a_1) \xi_n'^{(1)}(k_0 a_1) - \psi_n'(k_0 a_1) \xi_n'^{(1)}(k_0 a_1)} \right] \quad \text{(A.2)}$$

and

$$\bar{D}_{\nu\mu}^{nm(1,1)} = A_{\nu\mu}^{nm(1)} \left[\frac{(k_0/k_1) Z_{\nu n}^{(a)} \psi_n'(k_0 a_1) - Z_{\nu n}^{(c)} \psi_n(k_0 a_1)}{\xi_n^{(1)}(k_0 a_1) \psi_n'(k_0 a_1) - \xi_n'^{(1)}(k_0 a_1) \psi_n(k_0 a_1)} \right],$$

$$\bar{D}_{\nu\mu}^{nm(1,2)} = B_{\nu\mu}^{nm(1)} \left[\frac{(k_0/k_1) Z_{\nu n}^{(b)} \psi_n'(k_0 a_1) - Z_{\nu n}^{(d)} \psi_n(k_0 a_1)}{\xi_n{}^{(1)}(k_0 a_1) \psi_n'(k_0 a_1) - \xi_n'^{(1)}(k_0 a_1) \psi_n(k_0 a_1)} \right],$$

$$\bar{D}_{\nu\mu}^{nm(2,1)} = B_{\nu\mu}^{nm(1)} \left[\frac{(k_0/k_1) Z_{\nu n}^{(c)} \psi_n(k_0 a_1) - Z_{\nu n}^{(a)} \psi_n'(k_0 a_1)}{\xi_n'{}^{(1)}(k_0 a_1) \psi_n(k_0 a_1) - \xi_n^{(1)}(k_0 a_1) \psi_n'(k_0 a_1)} \right],$$

$$\bar{D}_{\nu\mu}^{nm(2,2)} = A_{\nu\mu}^{nm(1)} \left[\frac{(k_0/k_1) Z_{\nu n}^{(d)} \psi_n(k_0 a_1) - Z_{\nu n}^{(b)} \psi_n'(k_0 a_1)}{\xi_n'{}^{(1)}(k_0 a_1) \psi_n(k_0 a_1) - \xi_n^{(1)}(k_0 a_1) \psi_n'(k_0 a_1)} \right] \quad \text{(A.3)}$$

and

$$\begin{aligned} Z_{\nu n}^{(a)} &= [T_{\mathrm{HS},\nu}^{1} \xi_n^{(1)}(k_1 a_1) + \xi_n^{(2)}(k_1 a_1)], \\ Z_{\nu n}^{(b)} &= [T_{\mathrm{HS},\nu}^{2} \xi_n^{(1)}(k_1 a_1) + \xi_n^{(2)}(k_1 a_1)], \\ Z_{\nu n}^{(c)} &= [T_{\mathrm{HS},\nu}^{1} \xi_n'^{(1)}(k_1 a_1) + \xi_n'^{(2)}(k_1 a_1)], \\ Z_{\nu n}^{(d)} &= [T_{\mathrm{HS},\nu}^{2} \xi_n'^{(1)}(k_1 a_1) + \xi_n'^{(2)}(k_1 a_1)] \end{aligned} \quad \text{(A.4)}$$

The $A_{nm}^{\nu\mu(q)}$ and $B_{nm}^{\nu\mu(q)}$ are the translation coefficients needed for the transformation from the *i*th to the *k*th coordinate system [12]. They depend on the position vector, $\mathbf{r}_{ki}$, between the centers of the two spheres, and the amplitude of the local medium wavevector, k_1.

References

[1] W. Ross, Theoretical computation of light scattering power: comparison between TiO_2 and air bubbles, J. Paint Technol. 43 (563) (1971) 50–65.

[2] M. Kerker, D. Cooke, W. Ross, Pigmented microvoid coatings: theoretical study of three models, Paint Res. Inst. 47 (603) (1975) 33–41.

[3] C.F. Bohren, D.R. Huffman, Absorption and Scattering of Light by Small Particles, Wiley/Interscience, New York, 1983.

[4] P. Waterman, Symmetry unitary and geometry in electromagnetic scattering, Phys. Rev. D 3 (4) (1971) 825–839.

[5] P.W. Barber, S.C. Hill, Light scattering by particles: computational methods, Clarkson University, 1990.

[6] M.I. Mishchenko, L.D. Travis, A.A. Lacis, Scattering, Absorption and Emission of Light by Small Particles, Cambridge University Press, Cambridge, 2002.

[7] M. Kerker, The Scattering of Light, Academic Press, New York, London, 1969.

[8] F. Borghese, P. Denti, R. Saija, Optical properties of spheres containing a spherical eccentric inclusion, J. Opt. Soc. Am. A 9 (8) (1992) 1327–1335.

[9] G. Videen, D. Ngo, P. Chylek, R. Pinnick, Light scattering from a sphere with an irregular inclusion, J. Opt. Soc. Am. A 12 (5) (1995) 922–928.

[10] D. Ngo, G. Videen, P. Chylek, A FORTRAN code for the scattering of EM waves by a sphere with a nonconcentric spherical inclusion, Comput. Phys. Commun. 1077 (1996) 94–112.

[11] J.C. Auger, B. Stout, R.G. Barrera, F. Curiel, Scattering properties of rutile pigments located eccentrically within microvoids, JQSRT 70 (2001) 675–695.

[12] Stein, Addition theorems for spherical wave functions, Quart. Appl. Math. 19 (1) (1961) 15–24.

[13] W. Wiscombe, Improve Mie scattering algorithms, Appl. Opt. 19 (9) (1980) 1505–1509.

[14] B. Stout, J.C. Auger, J. Lafait, A transfer matrix approach to local field calculations in multiple scattering problems, J. Mod. Opt. 49 (13) (2002).